# Supplementary Information

## Multifunctional graphene woven fabrics

Xiao Li[1], Pengzhan Sun[1], Lili Fan[1], Miao Zhu[1,2], Kunlin Wang[1], Dehai Wu[1], Yao Cheng[2,3] and Hongwei Zhu[1,2*]

[1]Department of Mechanical Engineering, Key Laboratory for Advanced Manufacturing by Materials Processing Technology, Tsinghua University, Beijing 100084, China
[2]Center for Nano and Micro Mechanics (CNMM), Tsinghua University, Beijing 100084, China
[3]Department of Engineering Physics, Tsinghua University, Beijing 100084, China

*Correspondence and requests for materials should be addressed to H.W.Z. (email: hongweizhu@tsinghua.edu.cn).

**This file includes:**

Method: Strength predication of GWFs

Fig. S1 | Raman spectra of the GWF.

Fig. S2 | GWFs from nickel mesh.

Fig. S3 | SEM images of the GWF/PDMS composites.

Fig. S4 | PDMS protected hollow channels of graphene micron-tubes.

Fig. S5 | Tunable packing density by post manipulation.

Fig. S6 | GWF/PDMS composite under 50% strain.

Fig. S7 | Light current density-voltage curve for a GWF/Si solar cell.

Fig. S8 | Structure schematics of the GWF.

Fig. S9 | Cross-sectional schematic of the etching process of a copper wire.

Fig. S10 | Reflection spectra of planar Si, GWF/Si, and G/Si.

Table S1 | Performance summary of typical GWF/Si solar cells (AM1.5, 80mW/cm$^2$).

## Strength predication of GWFs

It has been verified that the strength of woven fabric is improved due to the effects of the crossing points, where warp and weft ribbons interlace with each other [1]. When a fabric is under uniaxial tension, the inter-ribbon interactions at the crossing points are found to consist of two components, a pressure-dependent frictional component and a pressure-independent adhesive one, of which the former was proved to be dominant for traditional woven fabrics; however, in our case, the latter might be dominant due to the 2D conformal adhesion of GMRs at the crossing points.

To estimate the strength of the graphene non-woven fabric (GWF), a dual-yarn system is employed [1]. Two sets of yarn are interlaced with each other to form a self-locked planar fibrous system. Once woven into fabric network, yarns will behave differently due to interactions at the crossing points, leading to the enhancement of the strength of the fabric network. Fig. S8 identifies the key geometrical parameters of the GWF. To evaluate the fabric and yarn properties, a critical length, $l_c$ is introduced.

As the contact area between yarns is only partial, when an external tension $\sigma$ is increased to the current tensile breaking load of the yarn, a force equilibrium can be established as:

$$\frac{C}{2L}\tau l_c = \sigma \tag{1}$$

where $h$ and $W$ are the shorter and longer axes of the yarn cross section, respectively. $\tau$ is the shear resistance. $L$ is the distance between adjacent yarns. $C$ is the circumference of the yarn cross section,

$$C = \frac{1.51\pi(h+W)}{2} - \frac{\sqrt{(hW)}}{2} \tag{2}$$

So, $C/2$ is the actual contact length between yarns, for one contact point. While in our GWF, graphene micron-ribbons (GMRs) are flattened, $h$ is close to zero. Therefore, $C$ is simplified as

$$C = 0.755\pi W \tag{3}$$

The actual fragment lengths are not a constant and vary in the range $l_c/2$ to $l_c$ and it is replaced by the mean fragment length $3l_c/4$. Because of the strong strength-length dependence of GMRs, the strengths of these segments will become higher owing to their shorter lengths.

The mean value of breaking load $\overline{\sigma}$ can be calculated as:

$$\overline{\sigma} = (L\alpha)^{-(1/\beta)}\Gamma(1+\frac{1}{\beta}) \tag{4}$$

where $\Gamma$ is the Gamma function, $\alpha$ is the Weibull scale parameter, and $\beta$ is the shape parameter of the yarn. Combining Eqs. (1), (3) and (4) gives

$$l_c = \left[\frac{0.84L}{W\tau}\left(\frac{4}{3}\alpha\right)^{-\frac{1}{\beta}}\Gamma\left(1+\frac{1}{\beta}\right)\right]^{\beta/(1+\beta)} \tag{5}$$

When pulling a yarn out of the network, a certain force is required to overcome the resistances between the contact points. There exist two components of the shear traction $\tau$ which resists any attempt of relative yarn movement at the contact area. One is pressure-independent adhesive force termed $\tau_2$, and the other is pressure-related frictional force $\tau_1$ ($\tau = \tau_1 + \tau_2$). Assume the network is under biaxial loading where the load $\sigma_L$ is applied in the warp direction and the load $\sigma_T$ in the weft direction. These external loads will create a pressures $P$, which will cause a frictional force $\mu P$. The frictional force is balanced by

$$\tau_1 C_0 = \mu P \tag{6}$$

$P$ can be calculated as

$$P = (2\sigma_T \sin\theta_T + 2\sigma_L \sin\theta_L) \tag{7}$$

where $\theta_i$, (i = T, L) are the interlacing angles at the longitudinal and transverse directions, respectively. In the GWF, as $\theta_i$ is extremely small, so is $P$, as a result $\tau_1$ is small.

The second component of $\tau$ can be calculated as:

$$\tau_2 = \frac{2\tau_s W}{C\rho} \tanh \rho W \tag{8}$$

where $\tau_s$ is defined as the elastic shear strength of the contact area, and $\rho$ is a factor reflecting the geometrical and mechanical properties of the graphene yarn:

$$\rho = \frac{2}{h}\sqrt{\frac{G}{\pi E}} \tag{9}$$

where *G/E*, is the ratio of the longitudinal shear modulus and tensile modulus of the graphene yarn. Combining Eqs. (3), (8) and (9) gives

$$\tau_2 = 0.42\tau_s h \sqrt{\frac{\pi E}{G}} \tanh 2\frac{W}{h}\sqrt{\frac{G}{\pi E}} \tag{10}$$

$\tau_2$ value is determined by the yarn mechanical properties *G/E*, and the geometrical property $\frac{W}{h}$. As $\frac{W}{h}$ is extremely large and $h \to 0$, $\tau_2$ is also small.

To conclude, $\tau = \tau_1 + \tau_2$ is small, but as $\tau > 0$, there also existence resistances to external loads to a certain degree. While because of the strong strength-length dependence of GMRs, the strengths of these segments will become higher owing to their shorter lengths. In conclusion, the strength of the GWF is higher than pure graphene sheets.

[1] Pan, N. Analysis of woven fabric strengths: Prediction of fabric strength under uniaxial and biaxial extensions. Compos. Sci. Technol. 56, 311-327 (1996).
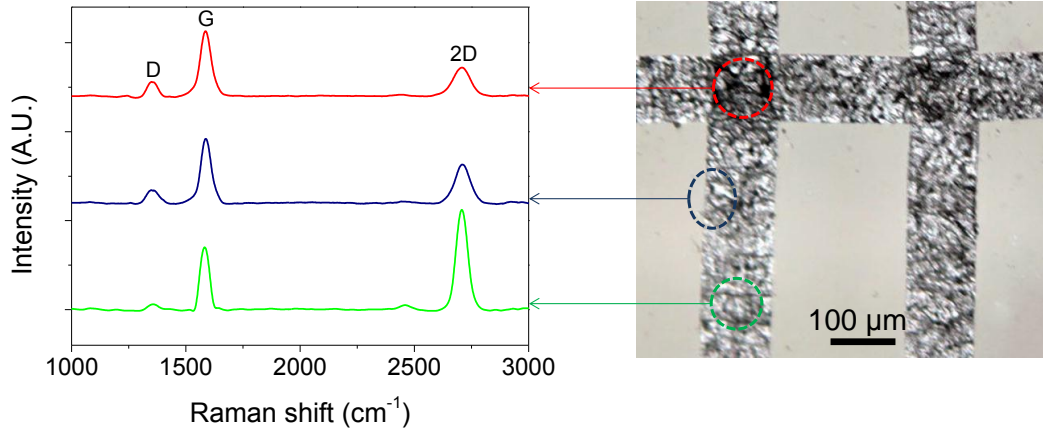


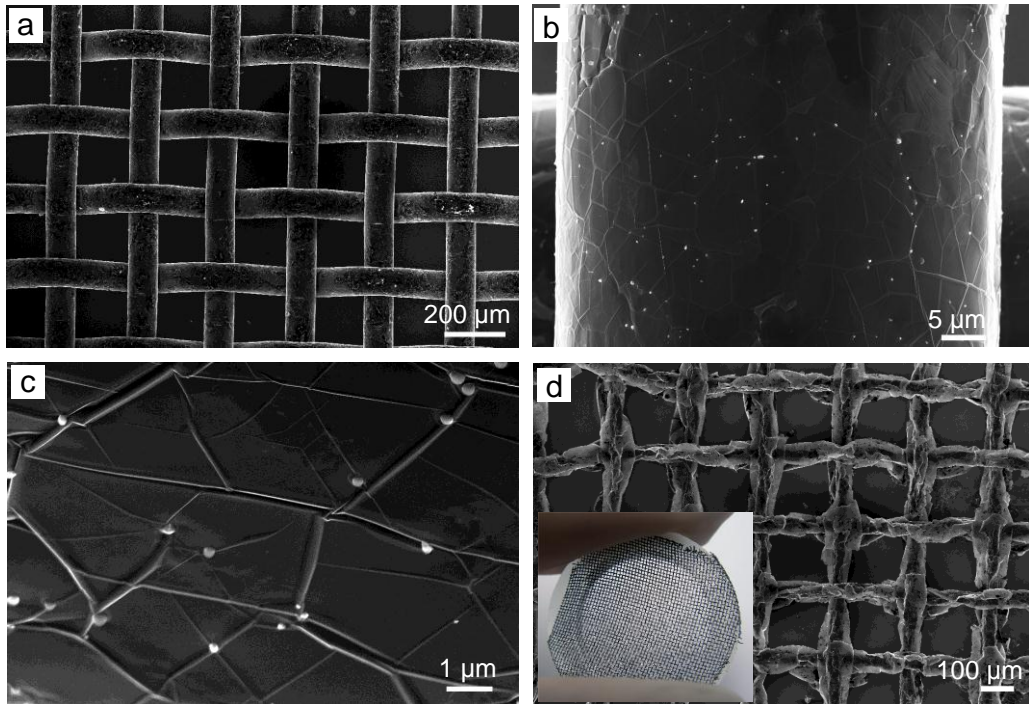Fig. S1 | Raman spectra of the GWF. Left panel shows an optical image with the marked regions.

Fig. S2 | GWFs from nickel mesh. (a) SEM image of nickel mesh after CVD growth. (b,c) Enlarged view SEM images of graphene grown on a nickel wire. (d) GWF obtained after nickel etching. Inset: GWF suspended over a quartz O-ring.
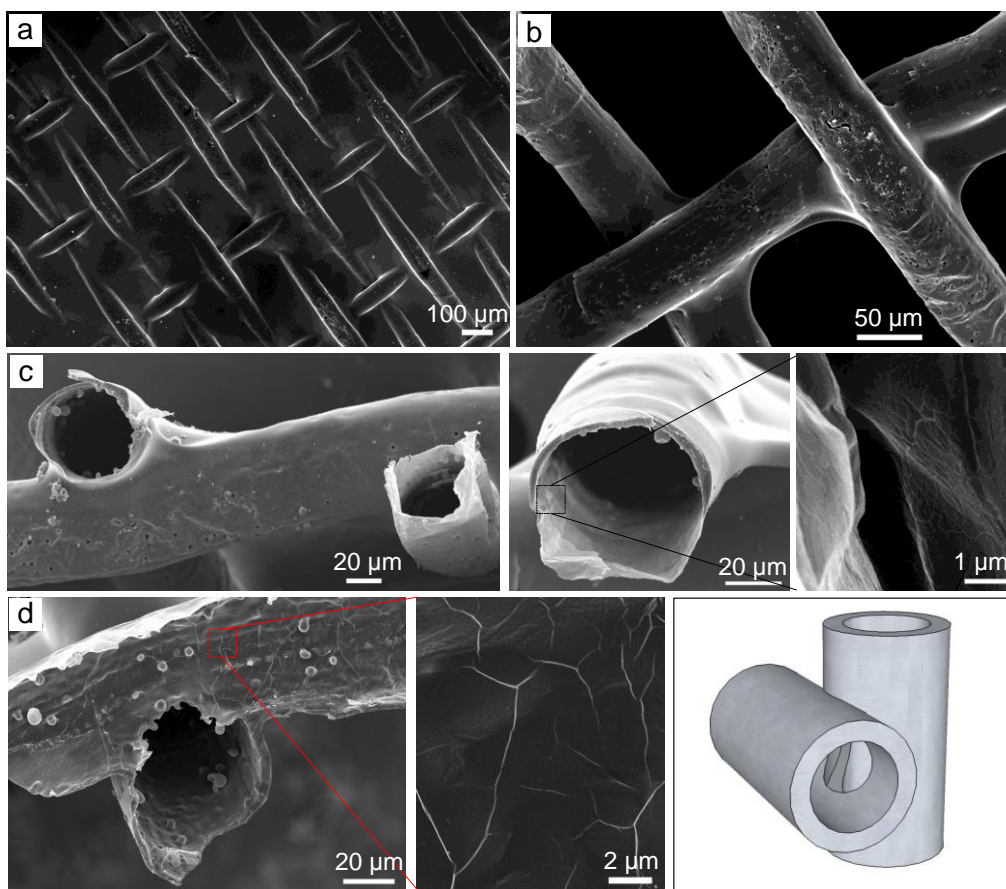
Fig. S3 | SEM images of the GWF/PDMS composites. (a) PDMS filled. (b) PDMS coated. (c) Cross-section view. (d) Multi-joint structure.
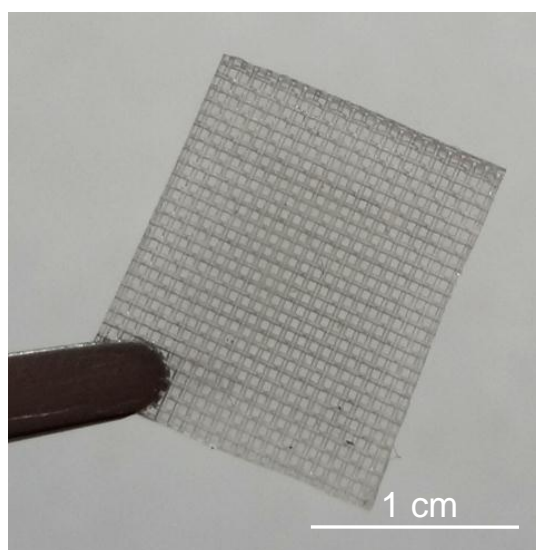


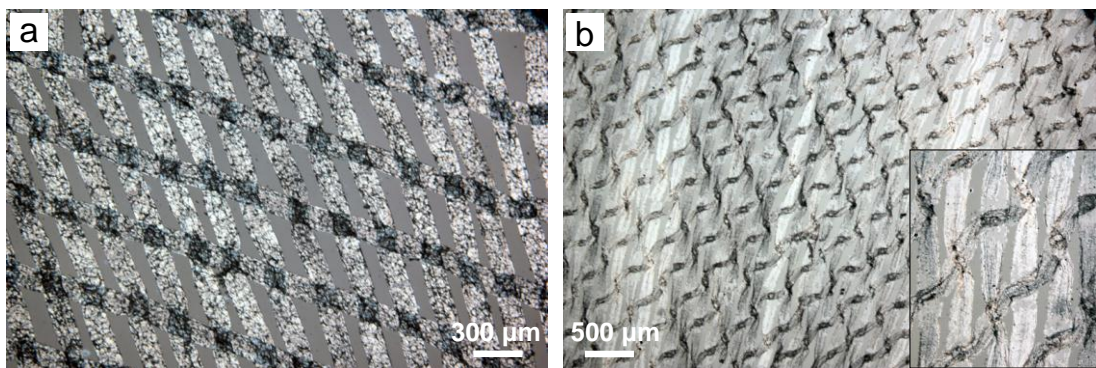Fig. S4 | PDMS protected hollow channels of graphene micron-tubes.

Fig. S5 | Tunable packing density by post manipulation. (a) Shear deformation. (b) Wavy deformation.
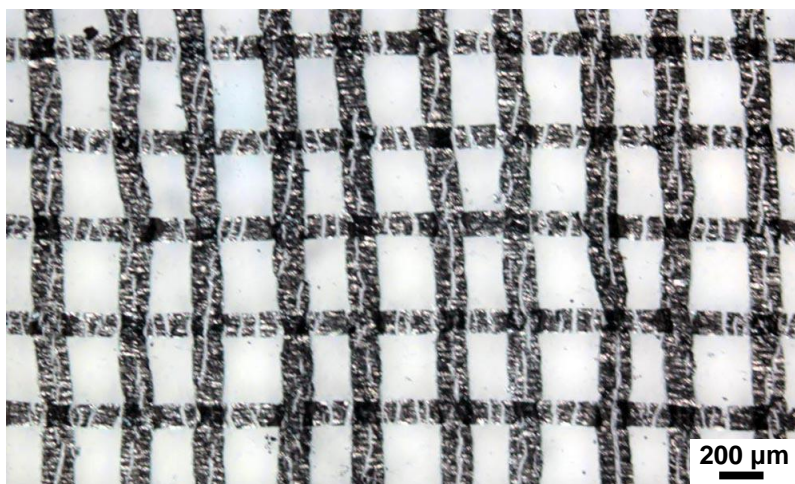


Fig. S6 | GWF/PDMS composite under 50% strain, showing cracks upon tensile test.



$V_{oc}$=0.50 V

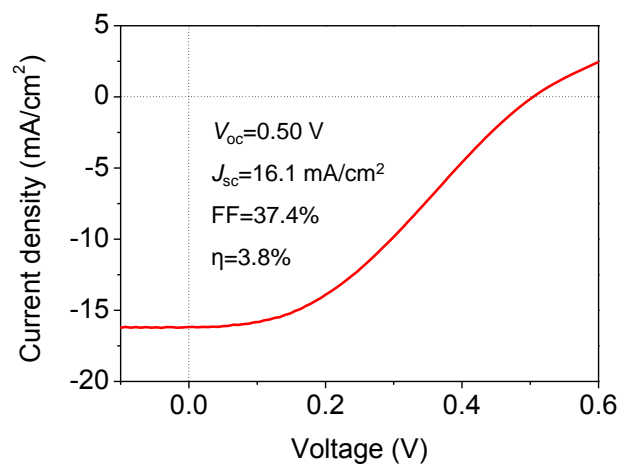$J_{sc}$=16.1 mA/cm$^2$

FF=37.4%

η=3.8%

Fig. S7 | Light current density-voltage curve for a GWF/Si solar cell.
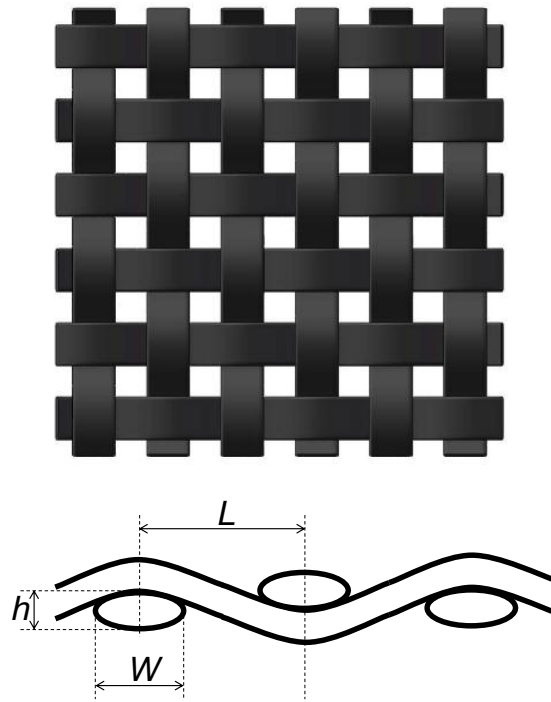
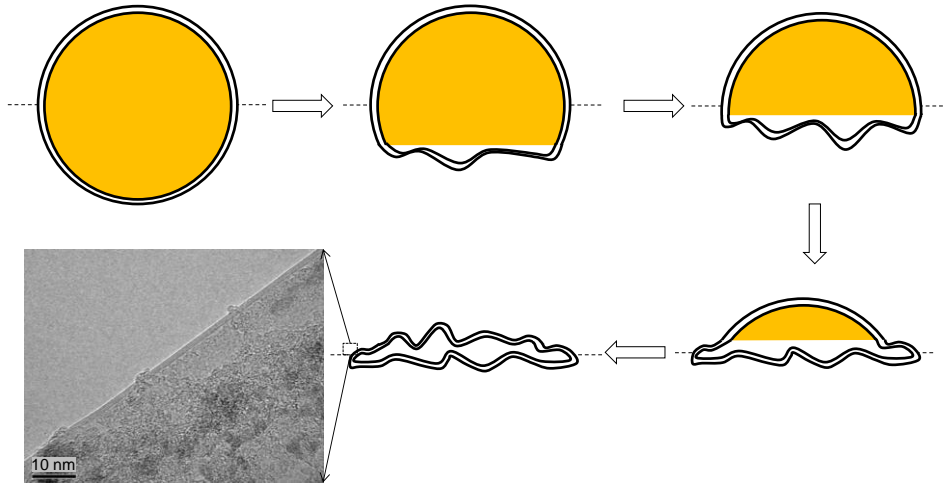Fig. S8 | Structure schematics of the GWF.



Fig. S9 | Cross-sectional schematic of the etching process of a copper wire.
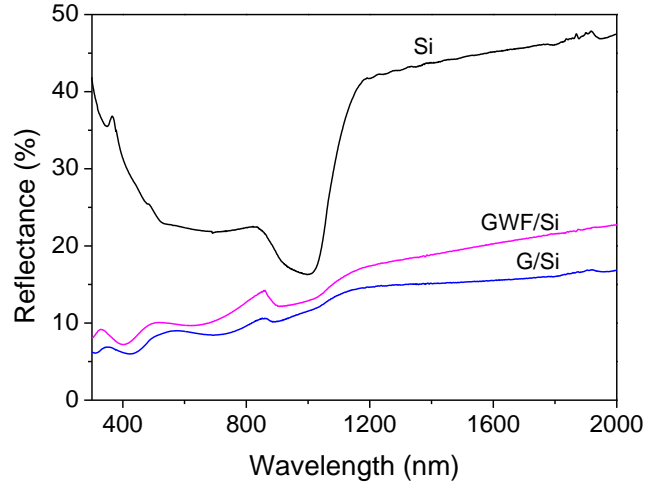
Fig. S10 | Reflection spectra of planar Si, GWF/Si, and G/Si.

Table S1 | Performance summary of typical GWF/Si solar cells (AM1.5, 80mW/cm$^2$).

| Samples | $V_{oc}$ (V) | $J_{sc}$ (mA/cm$^2$) | FF (%) | $\eta$ (%) |
|---|---|---|---|---|
| GWF-Si | 0.50 | 16.1 | 37.4 | 3.8 |
| GWF-Si HNO$_3$ before | 0.50 | 14.5 | 34.0 | 3.0 |
| GWF-Si HNO$_3$ after | 0.53 | 17.1 | 53.9 | 6.1 |
| GWF-Si PEDOT before | 0.35 | 18.3 | 30.9 | 2.5 |
| GWF-Si PEDOT after | 0.42 | 18.4 | 37.1 | 3.6 |
| GWF-Si HBr/Br$_2$ before | 0.46 | 16.3 | 31.3 | 2.9 |
| GWF-Si HBr/Br$_2$ after | 0.50 | 16.6 | 36.8 | 3.8 |